Metal-insulator transition in a spin-orbital-lattice coupled Mott system: $K_2V_8O_{16}$

Sooran Kim,[1,2] Beom Hyun Kim,[1,*] Kyoo Kim,[1,2,†] and B. I. Min[1,‡]
[1]*Department of physics, PCTP, Pohang University of Science and Technology, Pohang 37673, Korea*
[2]*c_CCMR, Pohang University of Science and Technology, Pohang 37673, Korea*
(Received 16 October 2015; published 8 January 2016)

We have explored the underlying mechanism of the metal-insulator transition (MIT) in hollandite-type vanadate, $K_2V_8O_{16}$, which has a quasi-one-dimensional chain structure and undergoes the MIT and Peierls-like structural transition upon cooling. For this purpose, we have investigated its electronic and magnetic properties in comparison to those of $Rb_2V_8O_{16}$ that also undergoes the MIT but without the Peierls-like structural distortion. We have found that $K_2V_8O_{16}$ is a spin-orbital-lattice coupled Mott system and manifests the orbital-selective Mott transition. The interplay of on-site Coulomb interaction, the magnetic-exchange interaction, and the Jahn-Teller-type tetragonal distortion plays an essential role in driving the MIT of $K_2V_8O_{16}$, inducing the the charge ordering (CO) and orbital ordering of V t_{2g} bands. The CO of V^{3+} and V^{4+} occurs in separate chains, preserving the inversion symmetry of the crystal. The d_{xy} orbitals form the spin-singlet state along the chain direction. The Peierls-like distortion does not play an essential role in the MIT.

DOI: 10.1103/PhysRevB.93.045106

I. INTRODUCTION

The metal-insulator transition (MIT) in strongly correlated systems has been a central subject in modern condensed matter physics because of complex and intriguing physical properties originating from charge-spin-orbital-lattice coupled interactions. Indeed, many theoretical models have been proposed to understand the mechanism of the MIT, such as the Slater mechanism, the Peierls mechanism, the Mott-Hubbard picture, and Anderson localization [1,2]. However, some exotic MITs in transition-metal oxides might be explained not just by one picture but by the cooperation of more than one physics [3–7]. A typical example is the complex MIT in VO_2, which is believed to occur through the interplay of Mott physics and Peierls physics [3–5].

The hollandite-type vanadate, $K_2V_8O_{16}$, of our present interest also manifests the MIT and Peierls-like structural transition, upon cooling, as in VO_2. The MIT in $K_2V_8O_{16}$ is accompanied by not only the structural transition but also charge ordering (CO) and the spin-singlet state [8]. $K_2V_8O_{16}$ exhibits nominal mixed valence, with average electrons per V being 1.25 (V^{4+}: V^{3+} = 3:1). In addition, differently from VO_2 that has single chain of edge-shared octahedra, $K_2V_8O_{16}$ of hollandite-type structure has a double chain of edge-shared octahedra, making a quasi-one-dimensional (quasi-1D) column structure, as shown in Fig. 1. It crystallizes in the body-centered tetragonal structure ($I4/m$) at high temperature (T) above 170 K (HT-KVO). At around $T = 170$ K, it undergoes the structural transition concurrently with the MIT from a tetragonal to a monoclinic cell [8,9]. The space group of $K_2V_8O_{16}$ at low T (LT-KVO) is $I2/m$ with a supercell of $\sqrt{2}a_H \times \sqrt{2}a_H \times 2c_H$, where a_H and c_H are the lattice parameters of HT-KVO. The Peierls-like structure distortions, such as V-V dimerization and zigzag distortion of V atoms, were observed at low T [10]. Half of the edge-shared octahedra have V-V dimer distortions, while the other half have zigzag distortions, which is reminiscent of the arrangement of V atoms in the $M2$ phase of VO_2 [11,12].

The mechanism of the MIT in $K_2V_8O_{16}$ has been a subject of controversy. Isobe *et al.* [9] proposed that the MIT could be separated as two parts: the first-order MIT at high T accompanied by the structural transition from a tetragonal to another tetragonal insulator (Tetra-ST), and the second-order structural transition at low T from the tetragonal to a monoclinic insulator (Mono-ST). However, the roles of the Tetra-ST and the Mono-ST in driving the MIT have not been fully elucidated. Interestingly, by the substitution of Rb for K, the Mono-ST disappears for $x > 0.6$ in $K_{2-x}Rb_xV_8O_{16}$ [9]. Specifically, $Rb_2V_8O_{16}$ undergoes the MIT at $T = 220$ K, accompanied only by the Tetra-ST. Further, by the substitution of Ti for V, both the Tetra-ST and the Mono-ST were found to disappear for $y > 0.5$ in $K_2V_{8-y}Ti_yO_{16}$, suggesting that the mechanism of the MIT is correlated with the CO of V^{3+} and V^{4+} [9]. Also, Yamauchi *et al.* [13] proposed two different CO phases to explain the two-step transitions in the resistivity during the MIT, both of which were claimed to be the first-order transitions. On the other hand, based on x-ray absorption and x-ray photoemission spectroscopy analyses, Ishige *et al.* [14] claimed that the Peierls mechanism arising from V^{4+}-V^{4+} pairing would drive the MIT, and then the orbital ordering (OO) formed by d_{xy} and d_{yz} of V^{3+} would cause the monoclinic distortion.

There has been debate even on the ground state of $K_2V_8O_{16}$ too. The CO and spin-singlet states were suggested as the ground state, since the magnetic susceptibility exhibits sudden drop during the MIT [8–10,13–17]. The OO of strongly correlated d_{xy} was also reported to emerge based on a ^{51}V nuclear magnetic resonance (NMR) experiment [16]. The spin gap size was measured to be $\Delta = 182$ K [16]. However, the suggested CO patterns by different groups were not consistent with each other. One pattern assumed separate V^{3+} and V^{4+} chains in the double chain, as shown in Fig. 1 [8,10,14]. The spin-singlet pairs were assumed to appear along chains. The other pattern assumed a mixed V^{3+}-V^{4+} chain and V^{4+} only chain [15]. The local spin-singlet between V^{4+} ions

*Present address: RIKEN, Wako, Saitama 351-0198, Japan.
†kyoo@postech.ac.kr
‡bimin@postech.ac.kr

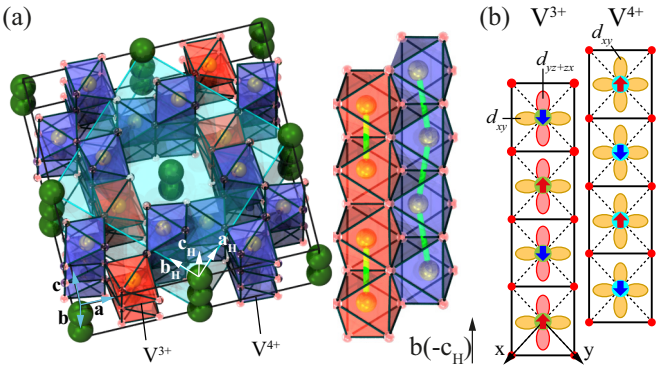

FIG. 1. (a) Left: The crystal structure of $K_2V_8O_{16}$. The blue box represents the unit cell of HT-KVO. Green, yellow, and red balls denote K, V, and O, respectively. The red and blue octahedra represents the V^{3+} and V^{4+} in the center, respectively. Right: The double chains of edge-shared VO_6 octahedra. The zigzag distortion is exaggerated as a guide. (b) The shape of occupied orbitals of V^{3+} and V^{4+} atoms. Red and blue arrows indicate the spin-up and spin-down local magnetic configurations, respectively. x and y represent local axes.

and local high-spin cluster were assumed to coexist in the same double chain. The latter mixed-chain model excludes the occupation of d_{xy}. Hence, the NMR result seemed to be more compatible with the former separate-chain model than with the latter mixed-chain model [16]. Even in the former separate-chain model, Komarek *et al.* [10] proposed a CO pattern that maintains the inversion symmetry of the crystal, whereas Ishige *et al.* [14] proposed a CO pattern that does not keep the inversion symmetry.

In contrast to so many experimental reports, there have been only a few theoretical reports on $K_2V_8O_{16}$. Sakamaki *et al.* [18] calculated the electronic structure of HT-KVO, and suggested a strong-coupling origin of the lattice instability based on the lack of a prominent nesting feature in the Fermi surface. Toriyama *et al.* [19] calculated the electronic structure of LT-KVO using the first-principle band method, but they could not capture either the insulating nature or the CO nature of LT-KVO even with the consideration of very large on-site Coulomb interaction.

In this paper, we have investigated the mechanism of the MIT and the ground state of $K_2V_8O_{16}$, which are compared with those of $Rb_2V_8O_{16}$. Using the first-principle band calculations, we have obtained the insulating electronic structures with CO and OO for both $K_2V_8O_{16}$ and $Rb_2V_8O_{16}$. We have demonstrated that the mechanism of the MIT is not the Peierls physics but the cooperative effects of the Mott physics, magnetic-exchange interaction, and the Jahn-Teller-type tetragonal distortion, causing the CO and OO nature.

II. COMPUTATIONAL DETAILS

We have used the VASP package, which implements the pseudopotential plane wave band method [20]. The generalized-gradient approximation (GGA) was utilized for the exchange-correlation energy. The effective on-site correlation, $U_{eff} = U - J = 3$ eV, was adopted, as in other vanadates [21–23]. For the double-counting correction in the GGA + U, the Dudarev method was used [24]. To simulate the local magnetic configuration of the spin-singlet state, the antiferromagnetic ordering between two spins was assumed [25,26]. We considered the antiferromagnetic (AF) ordering along the b axis and the in-plane ferromagnetic (FM) ordering, as shown in Fig. 1(b). This kind of magnetic configuration was discussed in the previous report [14].

The structural parameters of HT-KVO and LT-KVO were taken from experiments [10,27]. The initial lattice parameters of $Rb_2V_8O_{16}$ were adopted from the experiment [9], and, for atomic positions, those of $K_2V_8O_{16}$ were employed [27,28]. To consider the AF ordering, we used a $1 \times 1 \times 2$ supercell of $Rb_2V_8O_{16}$. Then the lattice parameters and atomic positions of $Rb_2V_8O_{16}$ were obtained after the full relaxation.

III. RESULTS

Figure 2 shows band structures of $K_2V_8O_{16}$ for different structures, on-site correlations, and magnetic configurations. We adopted the orthorhombic Brillouin zone (BZ), as shown in Fig. 2(e), because the monoclinic structure of LT-KVO has $\beta \sim 90^\circ$. Figure 2(a) shows the band structure of HT-KVO calculated in the GGA (HT-KVO-GGA), which is metallic, consistent with experiments [8,9] and previous calculation [18]. The t_{2g} bands are almost degenerate for HT-KVO. For LT-KVO in Fig. 2(b), which has Peierls-like structural distortions

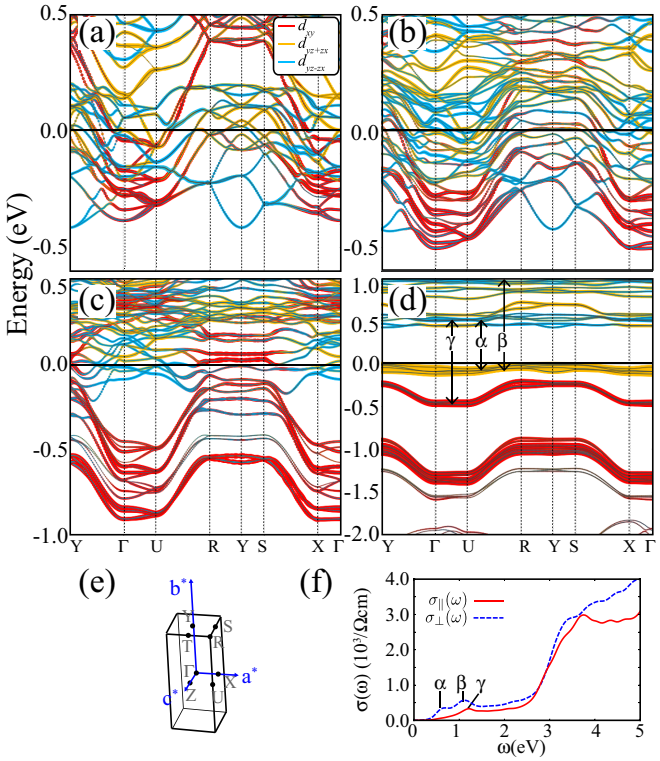

FIG. 2. Band structures of $K_2V_8O_{16}$ for various cases, plotted in the BZ of LT-KVO. (a) HT-KVO-GGA, (b) LT-KVO-GGA, (c) LT-KVO-GGA + U + NM, and (d) LT-KVO-GGA + U + AF. (e) The BZ of LT-KVO. (f) The optical conductivity $\sigma_{\parallel}(\omega)$ (parallel to the chain direction) and $\sigma_{\perp}(\omega)$ (perpendicular to the chain direction) of LT-KVO-GGA + U + AF.

such as V-V dimer and zigzag distortion, the metallic band structure is still obtained in the GGA (LT-KVO-GGA), in disagreement with experiments [8,9]. The 3D band feature manifested in HT-KVO of Fig. 2(a) is not much changed. The band gap does not open at the zone boundary, R-Y-S plane at $\pi/b \sim \pi/2c_H$, formed by Peierls dimerization (c_H is the lattice parameter of HT-KVO along the chain direction). This result suggests that $K_2V_8O_{16}$ is not a simple band or Peierls insulator.

We considered on-site Coulomb correlation U of V $3d$ electrons to describe the insulating ground state of LT-KVO in its nonmagnetic (NM) phase (LT-KVO-GGA + U + NM). Then the t_{2g} orbital degeneracy is lifted to separate downward the d_{xy} orbital, as shown in Fig. 2(c). Note that the bands are mostly flat in the entire BZ, except along the chain direction, b^*. This implies that, with consideration of U, the electrons are localized in the ac plane, and the crystal exhibits one-dimensionality along the chain direction, b. However, even the GGA + U band structure in Fig. 2(c) cannot capture the insulating nature of LT-KVO, as in a previous theoretical report [19].

The reported spin-singlet state in LT-KVO suggests that a magnetic-exchange interaction, such as short range AF interaction, could be important in this system. Hence we considered the AF ordering as an approximation of the local spin-singlet configuration [25,26]. Indeed, in the GGA + U calculation for LT-KVO with the AF configuration (LT-KVO-GGA + U + AF), we successfully obtained the insulating state with a gap size of ~0.4 eV, as shown in Fig. 2(d). In fact, this is the first theoretical description of insulating electronic structure of LT-KVO. V t_{2g} bands near the Fermi level (E_F) are almost localized in the entire BZ. Only $3d_{xy}$ orbitals are slightly dispersive along the chain direction, reflecting the 1D nature of the system. We checked that just the GGA calculation for LT-KVO with the AF configuration does not produce the insulating state, which implies that the MIT in $K_2V_8O_{16}$ is driven by the cooperation of the Mott physics and the magnetic-exchange interaction. Furthermore, LT-KVO with consideration of U and FM interaction also exhibits the insulating behavior, which rules out the Slater-type mechanism for the MIT.

Figure 2(f) shows the calculated optical conductivities $\sigma_{\parallel}(\omega)$ parallel to the chain direction and $\sigma_{\perp}(\omega)$ perpendicular to the chain direction. The spectra below 3 eV originate from the d-d interband transitions among t_{2g} bands, as shown in Fig. 2(d). The α peak in $\sigma_{\perp}(\omega)$ corresponds to the energy gap obtained from the band structure. $\sigma_{\parallel}(\omega)$ shows the peak near 1 eV, which corresponds to the excitation from the d_{xy} orbital that is directed along the chain. The spectra above 3 eV come from not only p-d interband transition but also intersite d_{xy}-d_{xy} and d_{yz+zx}-d_{yz+zx} interband transitions [see Figs. 3(e) and 3(f)]. These interband transitions are related to the hopping channels yielding the AF interaction.

To examine the local electronic structure in $K_2V_8O_{16}$, we analyzed its partial density of states (PDOS) in Fig. 3. The PDOS in Fig. 3(a) for HT-KVO-GGA does not show any feature of CO or OO. The d_{xy} state is more occupied than d_{yz+zx} and d_{yz-zx}, but they are almost in the same energy range, and so the occupancy of each state is more or less similar.

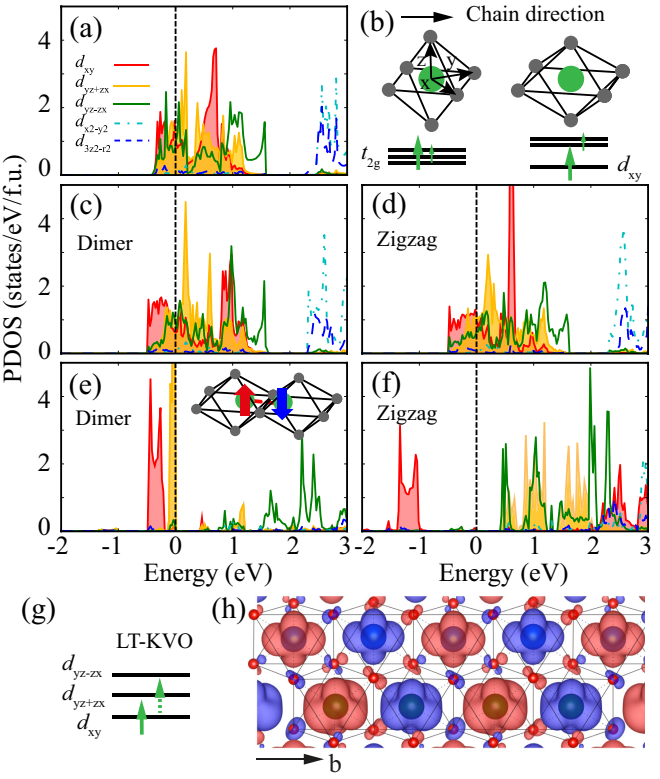

FIG. 3. (a) V $3d$ PDOSs for HT-KVO-GGA. The local axes are presented in (b). (b) The effect of Jahn-Teller-type tetragonal distortion on the V t_{2g} energy levels. Left: energy levels in the VO_6 octahedron of HT-KVO. Right: energy levels in the tetragonally distorted VO_6 octahedron. The small arrow corresponds to the electron number of 0.25. (c) V $3d$ PDOSs for V forming V-V dimer for LT-KVO-GGA. (d) V $3d$ PDOSs for V forming V-V zigzag distortion for LT-KVO-GGA. (e) V $3d$ PDOSs for V in the V^{3+}-V^{3+} dimer chain for LT-KVO-GGA + U + AF. The inset shows two edge-shared octahedra with AF spin configuration. (f) V $3d$ PDOSs for V in the V^{4+}-V^{4+} zigzag chain for LT-KVO-GGA + U + AF. (g) V t_{2g} energy levels in LT-KVO. The dotted green arrow represents the electron only for V^{3+}. (h) The spin density of double chain of V^{3+} and V^{4+} edge-shared octahedra. Red and blue isosurfaces are for spin up and down, respectively.

The main difference between the structures of HT-KVO and LT-KVO is the V-V dimer and the zigzag distortion of V in the latter. We found that the tetragonal distortion of the VO_6 octahedron, as shown in Fig. 3(b), is another important difference between two. The tetragonal distortion is consistent with the Tetra-ST, because the lattice constant along the chain direction increases after the Tetra-ST [9]. Specifically, the tetragonal distortions of VO_6 octahedra are pertinent to the Tetra-ST, while the V-V dimer and the zigzag distortion of V are pertinent to the Mono-ST. Because of the tetragonal distortion, the occupancy of the d_{xy} state would increase due to lowered d_{xy} energy level, as shown in Fig. 3(b). Indeed, Figs. 3(c) and 3(d) for the dimer and zigzag chains, respectively, of LT-KVO-GGA show such a tendency of increased d_{xy} occupancy. Thus, the tetragonal distortion plays a similar role of Jahn-Teller-type distortion so as to induce the OO of d_{xy}. The consideration of on-site Coulomb correlation

enhances the d_{xy} occupancy further for all chains (data are not shown). However, the insulating nature of LT-KVO cannot be captured in the GGA + U as well as in the GGA, which implies that just the lattice distortions are not sufficient to drive the MIT of $K_2V_8O_{16}$.

One may expect that the degeneracy lift of d_{xy} originates from the dimerization or zigzag distortion, but not from the tetragonal distortion. However, the PDOS of hypothetical structure of LT-KVO without Peierls-like distortions also exhibits the increased d_{xy} occupancy. In comparison to the GGA calculation for M2-VO_2 [11], the bonding-antibonding feature of the dimer chain or the OO feature in d_{xy} of the zigzag chain is much reduced in the GGA calculation for LT-KVO. The difference between two systems can be understood from the difference in their internal atomic parameters. The length difference between long V-V bond and short V-V bond in a dimer chain of LT-KVO, 0.3 Å, is smaller than that of $M2$-VO_2, 0.7 Å, which indicates that the dimerization is much weaker in LT-KVO. The bond angle among V-O-V atoms in the zigzag chain of LT-KVO, 175°, is closer to 180° than that of $M2$-VO_2, 162° [10,29]. Therefore, the tendency of the Peierls-like instability would be much reduced in LT-KVO, suggesting that another mechanism would be necessary to describe the MIT.

As shown in Figs. 3(e) and 3(f), the insulating electronic structure with clear OO and CO feature is obtained by considering the magnetic-exchange interaction together with the on-site Coulomb interaction. The PDOS in Fig. 3(e) is for V^{3+}, forming dimer distortion in the V^{3+} chain of edge-shared octahedra, and that in Fig. 3(f) is for V^{4+} in the zigzag chain. The other half of dimer chains having V^{4+} shows similar PDOS to Fig. 3(f). Thus, in LT-KVO, the d_{xy} and d_{yz+zx} states are occupied for V^{3+}, while only the d_{xy} state is occupied for V^{4+}, as shown in Fig. 3(g). Note that the emergence of OO of d_{xy} and d_{yz+zx} in LT-KVO has never been pointed out before, to our knowledge. These d_{xy} and d_{yz+zx} orbitals are directed along the chain direction, b [See Fig. 1(b)]. The d_{xy} orbital becomes lower in energy because of the compressed tetragonal distortion along the z direction. The d_{yz+zx} orbital would be selected to reduce the Coulomb repulsion in the ac plane because the crystal structure shrinks in the ac plane and extends along the chain direction after the MIT [8,9,14]. It is seen in Figs. 3(e) and 3(f) that only those selective orbitals of d_{xy} and d_{yz+zx} undergo the Mott transitions, and so hereafter we call it orbital-selective Mott transition.

We examined the difference between LT-KVO and another hollandite, $K_2Cr_8O_{16}$. In the case of $K_2Cr_8O_{16}$, the d_{xy} orbital is already occupied; the important orbital relevant to the MIT is the in-plane d_{yz-zx} orbital rather than the chain-directed orbital [30,31]. The lattice parameters do not change much after the MIT in $K_2Cr_8O_{16}$ (only 0.03% elongation in the chain direction and 0.05% shrinkage in in-plane parameters) [32]. In contrast, for $K_2V_8O_{16}$, the lattice parameter along the chain direction extends by 0.9% and the in-plane lattice parameters shrink by 0.6% [8,10]. Therefore, the occupation of d_{yz+zx} in addition to already occupied d_{xy} is preferred in $K_2V_8O_{16}$, which brings about more 1D-like nature along the chain direction than in $K_2Cr_8O_{16}$.

The spin density plot in Fig. 3(h) shows the spin and orbital configurations in the double chain of V^{4+} (upper part) and V^{3+} (lower part) octahedra. This figure reveals that the AF interaction exists in between V along the intrachain direction, while both FM and AF interactions exist in between V along the interchain direction. The spin configuration of d_{xy} and d_{yz+zx} is schematically plotted in Fig. 1(b). The OO of d_{xy} with the AF interaction along the b axis indicates that d_{xy} orbitals would be involved in forming the spin-singlet state [16].

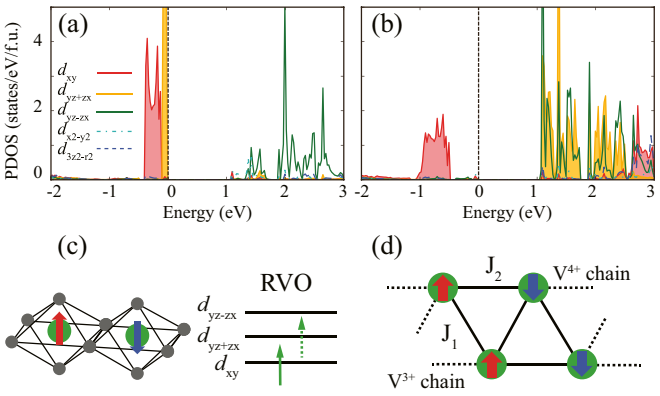

FIG. 4. (a) V 3d PDOSs for V^{3+} for LT-RVO-GGA + U + AF. (b) V 3d PDOSs for V^{4+} for LT-RVO-GGA + U + AF. (c) Left: edge-shared octahedra with the AF spin configuration. Right: V t_{2g} energy levels in the tetragonally distorted VO_6 octahedron of LT-RVO. The dotted green arrow represents the electron only for V^{3+} atom. (d) Spin configuration of V atoms in the double chain of edge-shared VO_6 octahedra. J_1 and J_2 represent interchain and intrachain magnetic-exchange parameters, respectively.

The obtained CO pattern shown in Fig. 1(a) is consistent with the separate chain model maintaining the inversion symmetry of the crystal [10]. The magnetic moments of V^{3+} and V^{4+} are calculated to be $\sim 1.78\mu_B$ and $\sim 1.04\ \mu_B$, respectively. These results suggest that the cooperation of CO and OO, which originate from the interplay among on-site Coulomb correlation, the magnetic-exchange interaction, and the Jahn-Teller-like distortion, plays an essential role in driving the MIT.

To examine the role of Peierls-like distortions of V-V dimer and zigzag formation in the MIT of $K_2V_8O_{16}$, we also investigated the electronic structure of $Rb_2V_8O_{16}$, which also crystallizes in the hollandite structure but without V-V dimer and zigzag distortion. The calculations were done for the relaxed structure of $Rb_2V_8O_{16}$. In fact, the structural optimization for $Rb_2V_8O_{16}$ results in the tetragonal distortions of VO_6 octahedra only, which corresponds to Tetra-ST for $K_2V_8O_{16}$ [9]. For $Rb_2V_8O_{16}$ too, the sharp reduction in magnetic susceptibility was observed, suggesting the spin-singlet formation after the MIT. Thus we considered not only the on-site Coulomb correlation and but also the AF configuration in the electronic structure calculation of $Rb_2V_8O_{16}$ (LT-RVO-GGA + U + AF). Figures 4(a) and (b) present the PDOSs of V^{3+} and V^{4+}, respectively, which reveal the insulating nature with CO and OO features in $Rb_2V_8O_{16}$. The energy gap of LT-RVO is obtained to be $\sim$1.1 eV. The d_{xy} and d_{yz+zx} are occupied for V^{3+}, while only d_{xy} is occupied for V^{4+}. The magnetic moments of V^{3+} and V^{4+} are obtained to

TABLE I. Equilibrium volumes and interchain (J_1) and intrachain (J_2) magnetic-exchange parameters, in units of eV, of LT-KVO and LT-RVO.

	LT-KVO GGA + U + AF	LT-RVO GGA + U + AF
Volume (Å^3)/f.u.	287.04	310.04
J_1	−0.012	−0.0074
J_2	0.026	0.0084
$\|J_2/J_1\|$	2.2	1.1

be $\sim 1.92\mu_B$ and $\sim 1.05\mu_B$. Note that these CO and OO are very similar to those in $K_2V_8O_{16}$. This finding suggests that the Peierls-like distortions do not have much effect on the formation of the CO or OO in the MITs of $Rb_2V_8O_{16}$ and $K_2V_8O_{16}$. The present result is different from that of Ishige *et al.* [14], which claimed that Peierls physics is the origin of MIT in $K_2V_8O_{16}$.

Figure 4(c) presents the t_{2g} energy levels under the tetragonal distortion of VO_6 and the spin configuration in LT-RVO. The lowest energy level of d_{xy} results only from the Jahn-Teller-type tetragonal distortion in LT-RVO, because LT-RVO does not have the Peierls-like distortions. The shrinkage of the in-plane direction and elongation of the chain direction were also detected in $Rb_2V_8O_{16}$ experimentally [9], which would be the reason for the occupation of the chain-directed d_{yz+zx} orbital in V^{3+}. The comparison of electronic structures of $Rb_2V_8O_{16}$ and $K_2V_8O_{16}$ thus reveals that the MITs in both systems show the orbital-selective Mott transitions, which arise from the cooperation of Coulomb correlation, magnetic-exchange interaction, and the Jahn-Teller-type tetragonal distortion, but not from the Peierls distortion.

Concerning the difference of $K_2V_8O_{16}$ and $Rb_2V_8O_{16}$ with and without Peierls-like distortions, we ascribed it to their volume difference. Because LT-RVO has larger volume than LT-KVO due to larger atomic size of Rb, as provided in Table I, the magnetic interaction in LT-RVO would be smaller than that in LT-KVO. To check this, we implemented the classical Ising-type spin Hamiltonian, $H = \Sigma_{i,j} J_{ij} S_i S_j$, where J_{ij} is the effective exchange interaction between two V spins. We set up the magnetic-exchange parameters, J_1 for the interchain and J_2 for the intrachain, as in Fig. 4(d). Each parameter was determined by the total-energy difference for different spin configurations. As we expected, J_1 and J_2 of LT-KVO are obtained to be larger than those in LT-RVO by 2–3 times, as provided in Table I. This means that the magnetic energy gain through the structural distortion would be small in $Rb_2V_8O_{16}$, which could be the reason for the nonexistence of Peierls distortion in $Rb_2V_8O_{16}$. In Fig. 4(d), it is noteworthy that, due to the triangle structure, the magnetic frustration states are expected to occur in both LT-KVO and LT-RVO.

IV. CONCLUSION

We have found that $K_2V_8O_{16}$ is a typical spin-orbital-lattice coupled Mott system. The MIT of the system occurs via the orbital-selective Mott transition. The insulating ground states of $K_2V_8O_{16}$ and $Rb_2V_8O_{16}$ arise from the cooperative interplay of Mott physics, magnetic-exchange interaction, and the Jahn-Teller-type tetragonal distortion, so as to induce the CO of V^{3+} and V^{4+} and the OO of d_{xy} and d_{yz+zx}. The obtained CO pattern keeps the inversion symmetry, which is consistent with one reported by Komarek *et al.* [10] The d_{xy} orbital is responsible for the formation of the spin-singlet state, which is consistent with the NMR experiment. We have separated the physics of MIT and Peierls-like distortions in $K_2V_8O_{16}$, demonstrating that the Peierls physics is not essential in driving the MIT. The absence of Peierls-like distortions in $Rb_2V_8O_{16}$ can be attributed to the strength difference of the local magnetic-exchange interactions. It is desirable to check our findings for $K_2V_8O_{16}$ and $Rb_2V_8O_{16}$ by using experimental tools such as time-resolved photoemission spectroscopy, pump-probe optical spectroscopy, and resonant x-ray scattering.

ACKNOWLEDGMENTS

This work was supported by the NRF of Korea (Grants No. 2011-0025237 and No. 2015R1A2A1A15053564), the Max-Plank POSTECH/KOREA Research Initiative (Grant No. KR 2011-0031558), and KISTI (Project No. KSC-2014-C3-044).

[1] M. Imada, A. Fujimori, and Y. Tokura, Rev. Mod. Phys. **70**, 1039 (1998).
[2] N. F. Mott, *Metal-Insulator Transitions* (Taylor and Francis, London, 1990).
[3] S. Biermann, A. Poteryaev, A. I. Lichtenstein, and A. Georges, Phys. Rev. Lett. **94**, 026404 (2005).
[4] M. W. Haverkort, Z. Hu, A. Tanaka, W. Reichelt, S. V. Streltsov, M. A. Korotin, V. I. Anisimov, H. H. Hsieh, H.-J. Lin, C. T. Chen, D. I. Khomskii, and L. H. Tjeng, Phys. Rev. Lett. **95**, 196404 (2005).
[5] S. Kim, K. Kim, C.-J. Kang, and B. I. Min, Phys. Rev. B **87**, 195106 (2013).
[6] R. Arita, J. Kunes, A. V. Kozhevnikov, A. G. Eguiluz, and M. Imada, Phys. Rev. Lett. **108**, 086403 (2012).
[7] S. Fujiyama, H. Ohsumi, T. Komesu, J. Matsuno, B. J. Kim, M. Takata, T. Arima, and H. Takagi, Phys. Rev. Lett. **108**, 247212 (2012).
[8] M. Isobe, S. Koishi, N. Kouno, J.-I. Yamaura, T. Yamauchi, H. Ueda, H. Gotou, T. Yagi, and Y. Ueda, J. Phys. Soc. Jpn. **75**, 073801 (2006).
[9] M. Isobe, S. Koishi, S. Yamazaki, J. Yamaura, H. Gotou, T. Yagi, and Y. Ueda, J. Phys. Soc. Jpn. **78**, 114713 (2009).
[10] A. C. Komarek, M. Isobe, J. Hemberger, D. Meier, T. Lorenz, D. Trots, A. Cervellino, M. T. Fernandez-Diaz, Y. Ueda, and M. Braden, Phys. Rev. Lett. **107**, 027201 (2011).
[11] V. Eyert, Ann. Phys. (Leipzig) **11**, 650 (2002).
[12] J. Pouget, H. Launois, T. Rice, P. Dernier, A. Gossard, G. Villeneuve, and P. Hagenmuller, Phys. Rev. B **10**, 1801 (1974).

[13] T. Yamauchi, H. Ueda, M. Isobe, and Y. Ueda, Phys. Rev. B **84**, 115104 (2011).
[14] Y. Ishige, T. Sudayama, Y. Wakisaka, T. Mizokawa, H. Wadati, G. A. Sawatzky, T. Z. Regier, M. Isobe, and Y. Ueda, Phys. Rev. B **83**, 125112 (2011).
[15] S. Horiuchi, T. Shirakawa, and Y. Ohta, Phys. Rev. B **77**, 155120 (2008).
[16] Y. Shimizu, K. Okai, M. Itoh, M. Isobe, J.-I. Yamaura, T. Yamauchi, and Y. Ueda, Phys. Rev. B **83**, 155111 (2011).
[17] K. H. Chow, M. Mansson, J. Sugiyama, O. Ofer, E. J. Ansaldo, J. H. Brewer, M. Isobe, H. Gotou, T. Yagi, Y. Ueda, and C. Baines, Phys. Procedia **30**, 117 (2012).
[18] M. Sakamaki, S. Horiuchi, T. Konishi, and Y. Ohta, arXiv:0811.4338.
[19] T. Toriyama, T. Konishi, and Y. Ohta, J. Phys. Conf. Ser. **400**, 032104 (2012).
[20] G. Kresse and J. Furthmüller, Phys. Rev. B **54**, 11169 (1996); Comput. Mater. Sci. **6**, 15 (1996).
[21] F. Mila, R. Shiina, F. C. Zhang, A. Joshi, M. Ma, V. Anisimov, and T. M. Rice, Phys. Rev. Lett. **85**, 1714 (2000).
[22] A. Liebsch, H. Ishida, and G. Bihlmayer, Phys. Rev. B **71**, 085109 (2005).
[23] W. E. Pickett, S. C. Erwin, and E. C. Ethridge, Phys. Rev. B **58**, 1201 (1998).
[24] S. L. Dudarev, G. A. Botton, S. Y. Savrasov, C. J. Humphreys, and A. P. Sutton, Phys. Rev. B **57**, 1505 (1998).
[25] Y. Guo, G. Zhang, X. Zhang, T. Jia, and Z. Zeng, J. Appl. Phys. **109**, 07E145 (2011).
[26] Y. Crespo, M. Fabrizio, S. Scandolo, and E. Tosatti, Proc. Natl. Acad. Sci. USA **111**, 10427 (2014).
[27] W. Abriel, F. Rau, and K.-J. Range, Mater. Res. Bull. **14**, 1463 (1979).
[28] The experimental atomic positions of $Rb_2V_8O_{16}$ have not been reported.
[29] M. Marezio, D. B. McWhan, J. P. Remeika, and P. D. Dernier, Phys. Rev. B **5**, 2541 (1972).
[30] S. Kim, K. Kim, and B. I. Min, Phys. Rev. B **90**, 045124 (2014).
[31] H. Takeda, Y. Shimizu, M. Itoh, M. Isobe, and Y. Ueda, Phys. Rev. B **88**, 165107 (2013).
[32] A. Nakao, Y. Yamaki, H. Nakao, Y. Murakami, K. Hasegawa, M. Isobe, and Y. Ueda, J. Phys. Soc. Jpn. **81**, 054710 (2012).